Supporting Information

A Conserved Glutamate Orchestrates Transitions Between Catalytic Intermediates in [NiFe]-Hydrogenase

Armel F. T. Waffo[a], Christian Lorent[a], Sagie Katz[a], Cornelius C. M. Bernitzky[b], Janna Schoknecht[a], Marius Horch[b], Oliver Lenz[a], Giorgio Caserta*[a] and Ingo Zebger*[a]

[a] *Institut für Chemie, Sekr. PC14, Technische Universität Berlin, D-10623 Berlin, Germany;*
[b] *Fachbereich Physik, Freie Universität Berlin, D-14195 Berlin, Germany;*

Corresponding Authors
*Giorgio Caserta, giorgio.caserta@tu-berlin.de
*Ingo Zebger, ingo.zebger@tu-berlin.de

Table of Contents

Table S1: Strains, plasmids and oligonucleotides used in this study.

Strain/plasmid	Relevant characteristics	Source/ reference
***C. necator* HF574**	*ΔhoxG*, *ΔhoxC*, *ΔhoxB*, *ΔhoxC*¸ MBH^-, RH^-, SH^-	[1]
***C. necator* HF574 (pGE567)**	RH_{Strep} overproduction	[1]
***C. necator* HF574 (pJS98)**	RH^{E13Q} ($HoxB_{Strep}HoxC^{E13Q}$) overproduction	This work
pCH1124	Amp, ColE1 *ori*, P_{SH}-$hoxB_{stop}$-Strep-tag II-*hoxC*	[1]
pEDY309	Tc^R , RK2 *ori*, Mob^+	[2]
pJS98	*Cn*RH E13Q, mutagenesis via Gibson assembly, 2.2 kb PCR product amplified with primers SFP96 and 2_#60_fw using pCH1124 as template, 3.3 kb PCR product amplified with primers #SFP95 and 4_#59_rev using pCH1124 as template, SpeI/HindIII-cut pEDY309	This work
Primers	Sequence (5´-3´)	
SFP96	CAGGCATCGTGGTGTCAC	*
2_#60_fw	GGTTCACCTCGAGGTCGCCCTGAACGCGGTTGAACGGC	*
SFP95	GCCATACCAAACGACGAGC	*
4_#59_rev	GCCGTTCAACCGCGTTCAGGGCGACCTCGAGGTGAACC	*

* Oligonucleotides were purchased from Sigma-Aldrich.

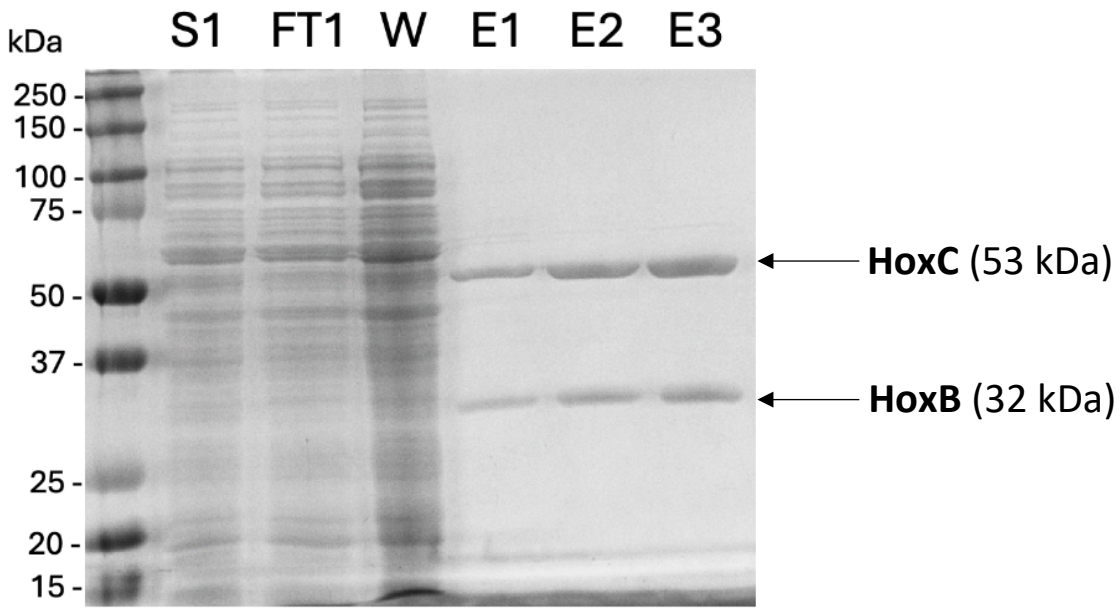

Figure S1: SDS-PAGE analysis of the RH^{E13Q} variant purified via Strep-Tactin affinity chromatography. Three different amounts of purified protein were loaded to the gel: E1 (2 µg), E2 (4 µg), and E3 (6 µg). The prominent band at approximately 53 kDa corresponds to the large subunit HoxC, while the smaller band at around 32 kDa represents the small subunit HoxB. Additional lanes include the supernatant of the cell lysate (S1), the flow-through (FT1), and the wash fraction (W). The Precision Plus Protein™ Dual Color Standard (BIO-RAD; range 250–15 kDa) served as molecular weight reference.

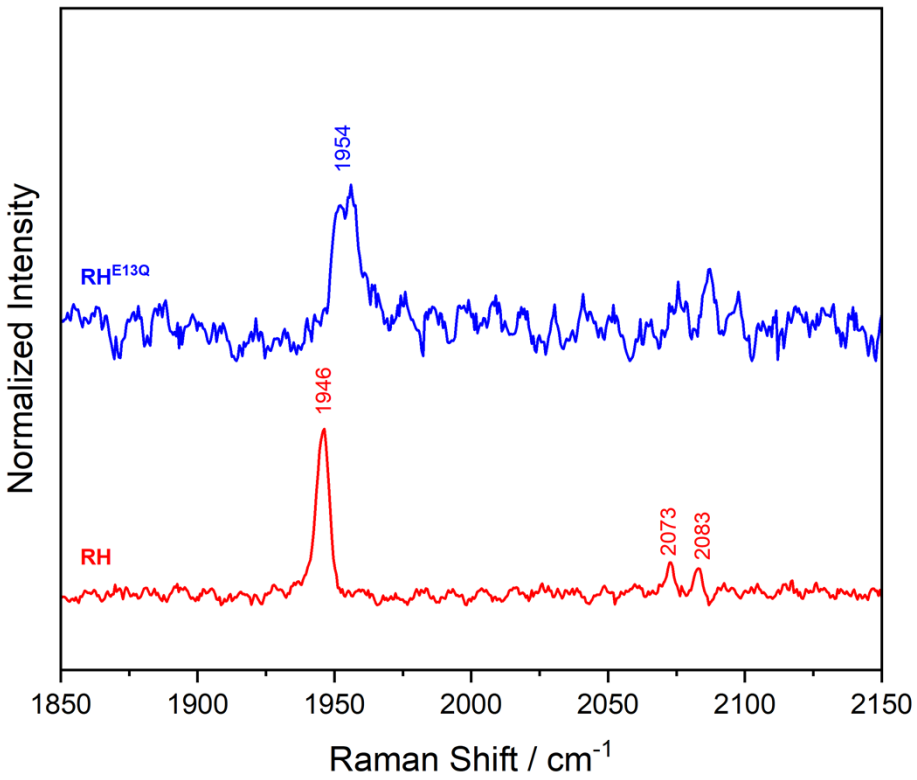

Figure S2: **Solution-phase resonance Raman spectra (80 K, excitation at 568 nm) of RH^{E13Q}** (top, blue) **and native RH** (bottom, red)**.** Spectra are normalized with respect to the intensity of the CO stretch band at 1954/1946 cm^{-1}. The data of native RH are reproduced from ref.[3]

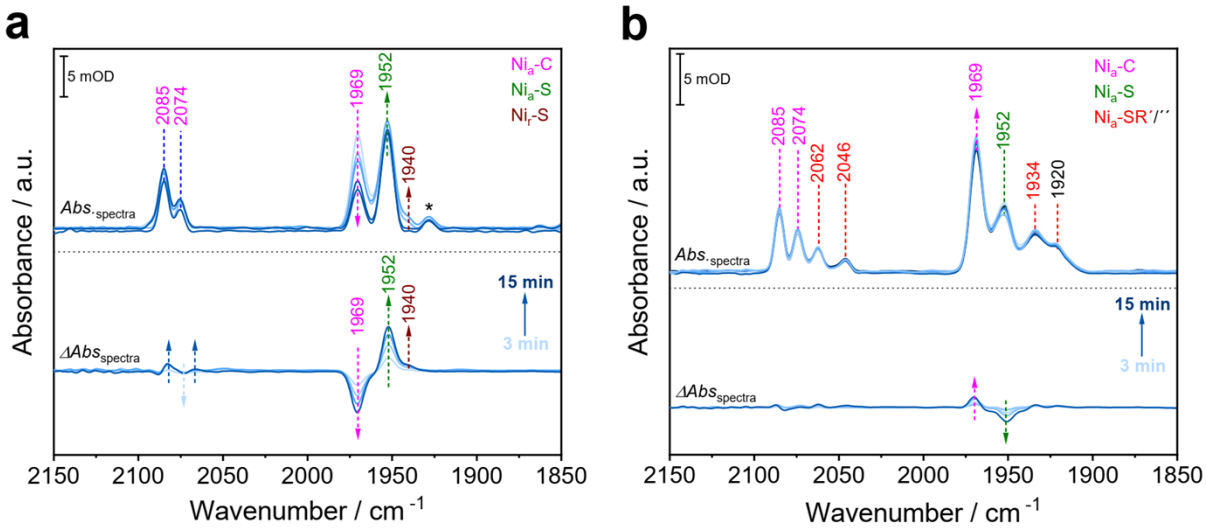

Figure S3: **Effect of the reduction protocol on the RH^{E13Q} variant.** IR absorbance spectra of RH^{E13Q}, recorded at 298 K after (**a**) treatment with H_2 alone and (**b**) with H_2 in the presence of sodium dithionite (NaDT). Panel (**a**) illustrates reoxidation events at the [NiFe] active site, where a significant portion of the reduced Ni$_a$-C state reverts to the Ni$_a$-S intermediate. The corresponding IR difference spectra (bottom) highlight the rapid conversion of the reduced Ni$_a$-C species back to the Ni$_a$-S state within minutes. In contrast, IR data of the H_2/NaDT-treated sample (**b**) show that RH^{E13Q} retains a reduced [NiFe] active site, which can be clearly visualized in the IR difference spectra (bottom). The ν_{CO} and ν_{CN} bands are labeled with their corresponding wavenumbers. * in **a** reflects traces of an unknown species. Ni$_a$-SR′/′′ subforms in **b** were enriched upon prolonged exposure of RH^{E13Q} to H_2 and NaDT (see also **Fig. 3**).

Table S2: Active site redox states observed for native RH and the RH^{E13Q} variant at different temperatures.

RH variant	Temp. (K)	Redox State	ν_{CO} (cm^{-1})	ν_{CN} (cm^{-1})	ν_{CN} (cm^{-1})	Ref.
native	298	Ni_r-B	1963	2097	2089	[4,5]
E13Q	298	Ni_r-B	1969	2096	n.d.	This work
native	298	Ni_a-S	1943	2080	2071	[2,6,7]
E13Q	298	Ni_a-S	1952	2084	2075	This work
native	90	Ni_a-S	1946	2082	2073	[7]
E13Q	90	Ni_a-S	1948	2082	2071	This work
E13Q	90	Ni_a-S^{Q}	1956	2086	2076	This work
native	298	Ni_a-SR	1948	2057	2047	[4,7]
native	298	Ni_a-SR´	1935	n.d.	n.d.	[8]
E13Q	298	Ni_a-SR	1956	2061	2045	This work
E13Q	298	Ni_a-SR´	1934	n.d.	n.d.	This work
E13Q	298	Ni_a-SR´´	1920	n.d.	n.d.	This work
native	298	Ni_a-C	1961	2082	2071	[4,7]
E13Q	298	Ni_a-C	1969	2085	2074	This work
E13Q	90	Ni_a-C	1967	2085	2072	This work
E13Q	90	Ni_a-C^{Q}	1972	2088	2074	This work
native	90	Ni_a-L1	1911	2056	2037	[7]
E13Q	90	Ni_a-L1	1915	2057	2035	This work
E13Q	90	Ni_a-L1^{Q}	1921	2061	2041	This work
native	90	Ni_a-L2	1914	2060	2044	[7]
E13Q	90	Ni_a-L2^{Q}	1917	n.d.	n.d.	This work

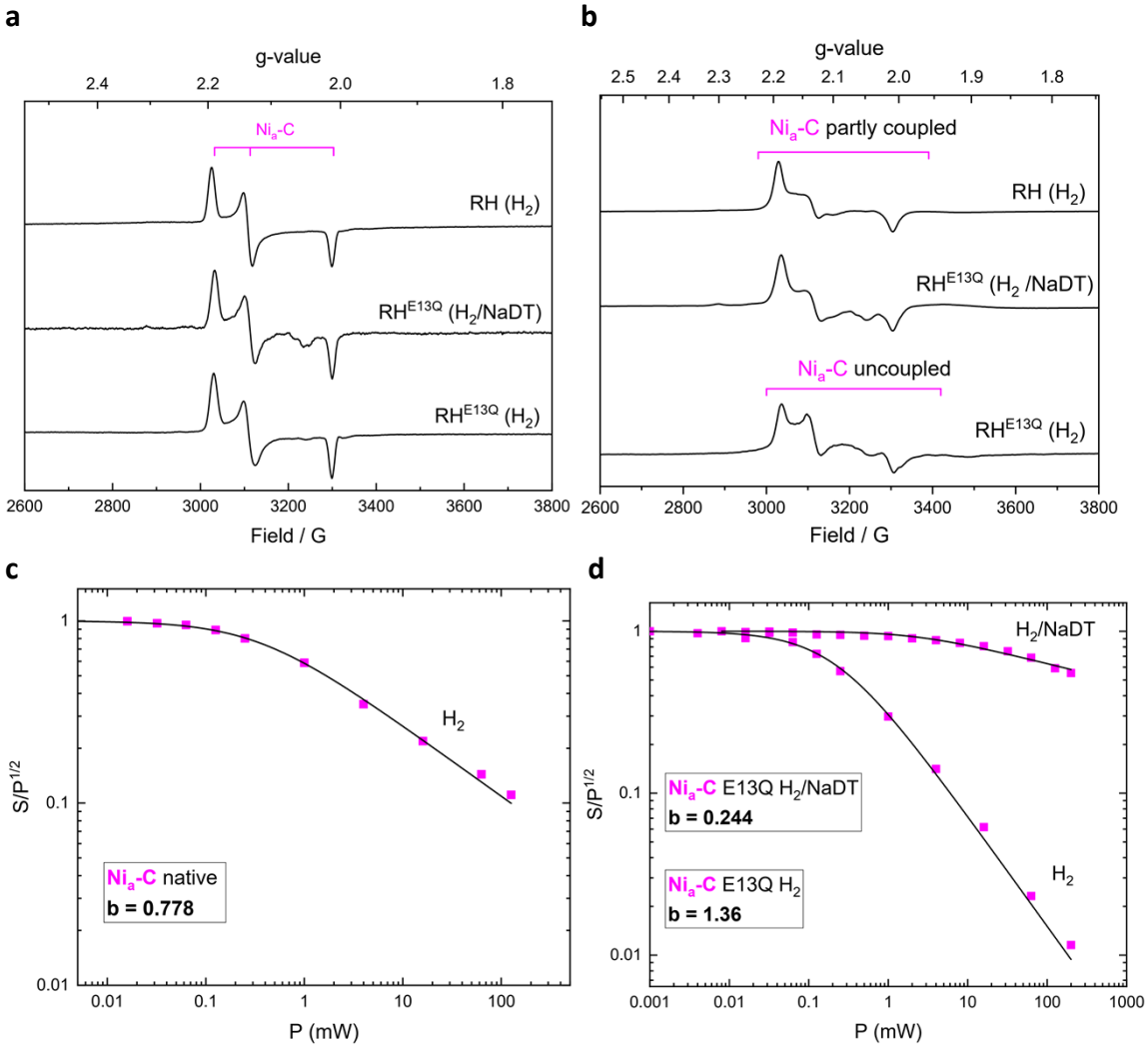

Figure S4. EPR spectra of reduced RH^{E13Q} and native RH and the corresponding power saturation data. EPR spectra recorded at 90 K (**a**) and 10 K (**b**). At temperatures below 10 K, the EPR spectrum of reduced native RH usually shows the characteristic broadening and partial splitting of the Ni$_a$-C signal and a distinct impact on the spin relaxation, which arises from the coupling with a nearby paramagnetic center, most likely the proximal [4Fe-4S] cluster.[9,10] Notably, EPR data of H$_2$-reduced RH^{E13Q} did not show these features, while it was observed for H$_2$/NaDT-reduced RH^{E13Q}. This suggests that the proximal [4Fe-4S]$^{1+}$ cluster remains mainly oxidized in H$_2$-reduced RH^{E13Q}. The power saturation curves for H$_2$-reduced native RH (**c**), H$_2$-reduced and H$_2$/NaDT-reduced RH^{E13Q} (**d**) recorded at 20 K agree with data in **b**. For H$_2$-reduced native RH ($P_{1/2}$ = 0.375 mW) and H$_2$/NaDT-reduced RH^{E13Q} ($P_{1/2}$ = 2.355 mW) a b-value < 1 was calculated indicating a dipolar coupling with a paramagnet in the vicinity, likely the proximal [4Fe-4S]$^{1+}$ cluster, while this coupling was absent (b > 1) for the H$_2$-reduced RH^{E13Q} because the cluster is likely in its 2+ oxidation state and thus diamagnetic ($P_{1/2}$ = 0.213 mW).[11,12]

Table S3. Fit parameters related to the light-driven Ni_a-C^Q/Ni_a-C to Ni_a-$L1^Q$/Ni_a-L1 conversion of RH^{E13Q} at 90 K.

Transition	k (s^{-1})	T (s)	A	R^2
Ni_a-$L1^Q$ formation	(4.08 ± 0.08) · 10^{-3}	244.9 ± 5.3	(-1.18 ± 0.01) · 10^{-2}	0.99
Ni_a-L1 formation	(4.68 ± 0.08) · 10^{-3}	213.7 ± 3.9	(-1.21 ± 0.01) · 10^{-2}	0.99
Ni_a-C^Q depletion	(4.20 ± 0.07) · 10^{-3}	238.3 ± 4.4	(1.20± 0.01) · 10^{-2}	0.99
Ni_a-C depletion	(4.99 ± 0.06) · 10^{-3}	200.3 ± 2.5	(1.24 ± 0.01) · 10^{-2}	0.99

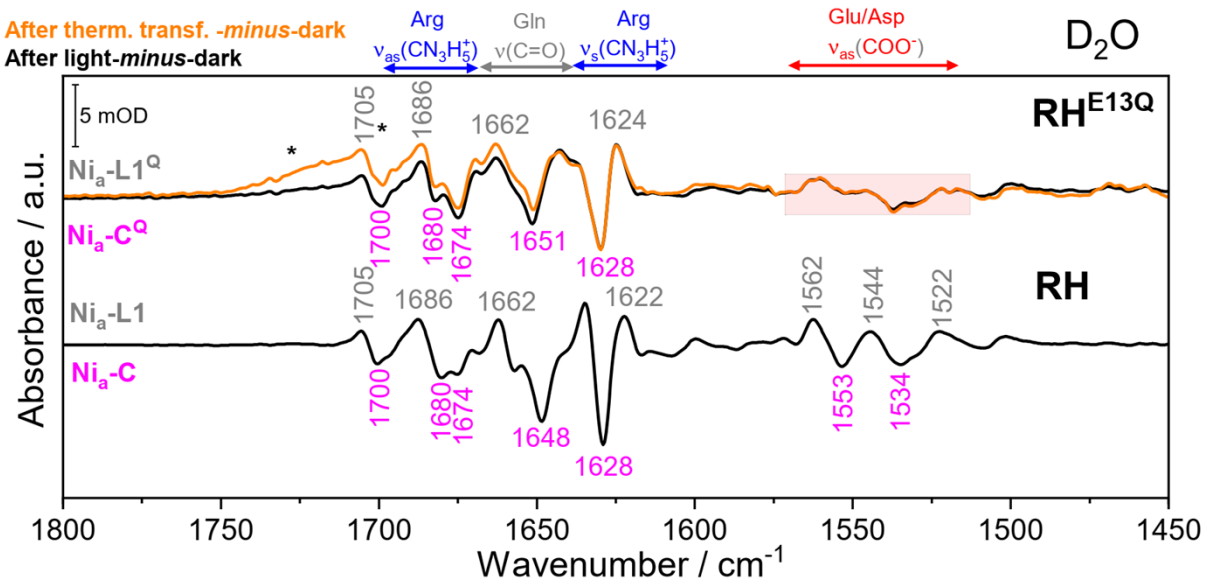

Figure S5: IR difference spectra of reduced native RH and RH^{E13Q} at 90 K in D_2O, revealing important elements of the first and outer coordination sphere of the corresponding [NiFe] sites. "After light-*minus*-dark" (black traces) and "after thermal transformation-*minus*-dark" (orange trace) difference spectra of native RH (bottom) and RH^{E13Q} (top) prepared in D_2/D_2O. The spectra in the range between 1800 and 1450 cm^{-1} show potential contributions from individual amino acid residues. The spectral regions characteristic for the main bands of arginine ($CN_3H_5^+$, ν_s and ν_{as}, blue arrow), glutamine ($\nu_{C=O}$, grey arrow) and deprotonated aspartate/glutamate (ν_{as} COO^-, red arrow), are highlighted. Amide I and amide II absorptions, which occur between 1600-1700 cm^{-1} and 1510-1580 cm^{-1}, respectively, may also contribute to the observed absorptions. We assign the broad band around 1700−1730 cm^{-1} (marked with *) to an artifact due to slight temperature fluctuations over time.

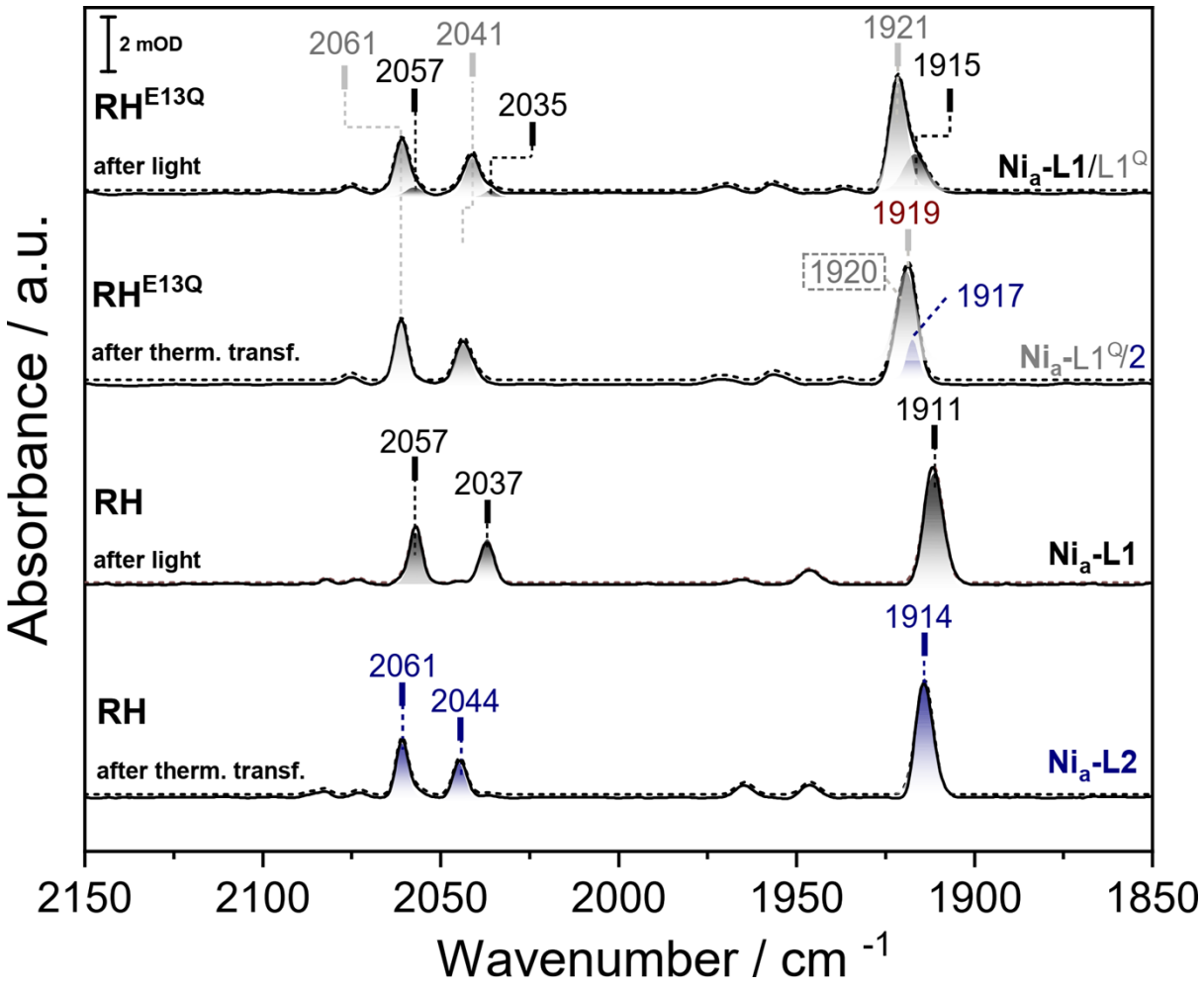

Figure S6. Low-temperature (90 K) IR absorbance spectra in the 2150–1850 cm^{-1} regime of H_2/NaDT-reduced RH^{E13Q} and native RH after illumination (after light) and after thermal transformation in the dark (after thermal transformation). The corresponding Gaussian fitting of the CO/CN bands are shown as dotted lines and include also traces of Ni_a-C/C^Q, Ni_a-S/S^Q species. While the 'after light' IR spectrum of native RH shows the enrichment of Ni_a-L1 (ν_{CO} at 1911 cm^{-1}), the corresponding IR spectrum of RH^{E13Q} exhibits absorptions of the Ni_a-L1 (ν_{CO} at 1915 cm^{-1}, minor species) and Ni_a-$L1^Q$ (ν_{CO} at 1921 cm^{-1}, major species). After thermal transformation, the RH spectrum displays exclusively signals corresponding to Ni_a-L2 (ν_{CO} at 1914 cm^{-1}), whereas the RH^{E13Q} IR spectrum shows only a minor contribution from Ni_a-L2 (approximately 20-30%, ν_{CO} at 1917 cm^{-1}), with the majority of the signal after relaxation still continuing to originate from Ni_a-$L1^Q$ (approximately 70-80%, ν_{CO} at 1920 cm^{-1}).

Supplementary References

[1] T. Buhrke, O. Lenz, N. Krauss, B. Friedrich, "Oxygen Tolerance of the H2-sensing [NiFe] Hydrogenase from Ralstonia eutropha H16 Is Based on Limited Access of Oxygen to the Active Site" *Journal of Biological Chemistry* **2005**, *280*, 23791–23796.

[2] L. Kleihues, O. Lenz, M. Bernhard, T. Buhrke, B. Friedrich, "The H_2 Sensor of *Ralstonia eutropha* Is a Member of the Subclass of Regulatory [NiFe] Hydrogenases" *J Bacteriol* **2000**, *182*, 2716–2724.

[3] C. C. M. Bernitzky, G. Caserta, S. Frielingsdorf, J. Schoknecht, A. Schmidt, P. Scheerer, O. Lenz, P. Hildebrandt, C. Lorent, I. Zebger, M. Horch, "Expanding the scope of resonance Raman spectroscopy in hydrogenase research: New observable states and reporter vibrations" *Journal of Inorganic Biochemistry* **2025**, *262*, 112741.

[4] P. A. Ash, J. Liu, N. Coutard, N. Heidary, M. Horch, I. Gudim, T. Simler, I. Zebger, O. Lenz, K. A. Vincent, "Electrochemical and Infrared Spectroscopic Studies Provide Insight into Reactions of the NiFe Regulatory Hydrogenase from *Ralstonia eutropha* with O_2 and CO" *J. Phys. Chem. B* **2015**, *119*, 13807–13815.

[5] G. Caserta, C. Lorent, A. Ciaccafava, M. Keck, R. Breglia, C. Greco, C. Limberg, P. Hildebrandt, S. P. Cramer, I. Zebger, O. Lenz, "The large subunit of the regulatory [NiFe]-hydrogenase from *Ralstonia eutropha* – a minimal hydrogenase?" *Chem. Sci.* **2020**, *11*, 5453–5465.

[6] A. J. Pierik, M. Schmelz, O. Lenz, B. Friedrich, S. P. J. Albracht, "Characterization of the active site of a hydrogen sensor from *Alcaligenes eutrophus*" *FEBS Letters* **1998**, *438*, 231–235.

[7] A. F. T. Waffo, C. Lorent, S. Katz, J. Schoknecht, O. Lenz, I. Zebger, G. Caserta, "Structural Determinants of the Catalytic Ni_a -L Intermediate of [NiFe]-Hydrogenase" *J. Am. Chem. Soc.* **2023**, *145*, 13674–13685.

[8] G. Caserta, K. Laun, J.-P. Oudsen, I. Sergueev, I. Zebger, O. Lenz, "NRVS Spectroscopy Resolves Distinct Bridging Hydride Intermediates in [NiFe]-Hydrogenase" *J. Am. Chem. Soc.* **2025**, *147*, 41216–41220.

[9] G. Caserta, C. Lorent, V. Pelmenschikov, J. Schoknecht, Y. Yoda, P. Hildebrandt, S. P. Cramer, I. Zebger, O. Lenz, "*In Vitro* Assembly as a Tool to Investigate Catalytic Intermediates of [NiFe]-Hydrogenase" *ACS Catal.* **2020**, *10*, 13890–13894.

[10] F. Roncaroli, E. Bill, B. Friedrich, O. Lenz, W. Lubitz, M.-E. Pandelia, "Cofactor composition and function of a H_2 -sensing regulatory hydrogenase as revealed by Mössbauer and EPR spectroscopy" *Chem. Sci.* **2015**, *6*, 4495–4507.

[11] D. J. Hirsh, G. W. Brudvig, "Measuring distances in proteins by saturation-recovery EPR" *Nat Protoc* **2007**, *2*, 1770–1781.

[12] H. Rupp, K. K. Rao, D. O. Hall, R. Cammack, "Electron spin relaxation of iron-sulphur proteins studied by microwave power saturation" *Biochimica et Biophysica Acta (BBA) - Protein Structure* **1978**, *537*, 255–269.